

Design of a plasmonic near-field tip for super-resolution IR-imaging

Fouad Ballout

*Department of Physics, Imperial College London, UK**

Erik Bründermann, Diedrich A. Schmidt, and Martina Havenith

Department of Physical Chemistry II,

Ruhr-Universität Bochum, Germany†

Abstract

The concepts of spoof surface plasmon polaritons and adiabatic field compression are employed to design metallic near-field probes that allow guiding and focusing of mid-infrared wavelength electromagnetic radiation and provides subwavelength field confinements and a lateral optical resolution of about 10 nm.

*Electronic address: f.ballout@imperial.ac.uk

†Electronic address: erik.bruendermann@rub.de

I. INTRODUCTION

In the past decades scattering scanning near-field microscopy (s-SNOM) in the infrared (IR) spectral region has become an established tool for imaging applications including electronic, polymeric and biological nanostructures. After a period of experimental showcases there is now a drive to increase its sensitivity and lateral resolution to a level where single molecule detection and imaging becomes accessible. However, owing to the long wavelength nature of the involved fields these efforts are limited, unless strategies are pursued that exploit the internal resonances of the sample and/or tip to enhance the coupling between the probe and the sample. Huber et al. [1–3] have utilized phonon polariton resonances of polar crystalline materials to achieve nonlinear field enhancements with a lateral resolution of 40 nm at IR and THz wavelengths. As a matter of fact, this approach is restricted to materials such as SiC, Si₃N₄, SiO₂ or III-V semiconductors (e.g. GaAs, InP) excluding all materials that do not exhibit phononic resonances including biological and soft materials.

In search of increased flexibility of s-SNOM the alternative approach [4] utilize the shape and internal resonances of the probe to excite surface plasmon polaritons (SPPs) that can concentrate the electromagnetic radiation into subwavelength regions [5, 6]. Unfortunately these resonances lie outside the chemical fingerprint region which limits the range of applications to optical wavelengths. In order to overcome these limitations, Pendry and co-workers [7, 8] suggested the introduction of a periodic arrangement of grooves and holes into the surface of a perfect electric conductor (PEC). This enforces the generation of SPP-like modes, so-called spoof SPP or designer SPP, at any any desired frequency in dependence of the periodicity. So far, this concept of designer SPP has been experimentally demonstrated in the microwave and THz regime [9–12]. Out of the number of theoretical investigations dealing with spoof SPPs [13–24] the work in Refs. [15, 18] is of most interest for the purpose of the work presented here as it utilizes spoof SPPs for THz microimaging. The authors proposed a periodically furrowed metallic tapered waveguide structure that focuses THz radiation down to the micrometer scale. In this paper we will pick up this strategy and present a novel design of a near-field nanotip which supports surface waves in the mid-IR wavelength domain between 5.7 and 6 μm , containing the dominant lipid and protein absorption bands, and focuses them down to the 10nm-scale. Our strategy is to find the grating parameters of a corrugated PEC wire to support spoof SPP modes in the wavelength range 5.7 - 6

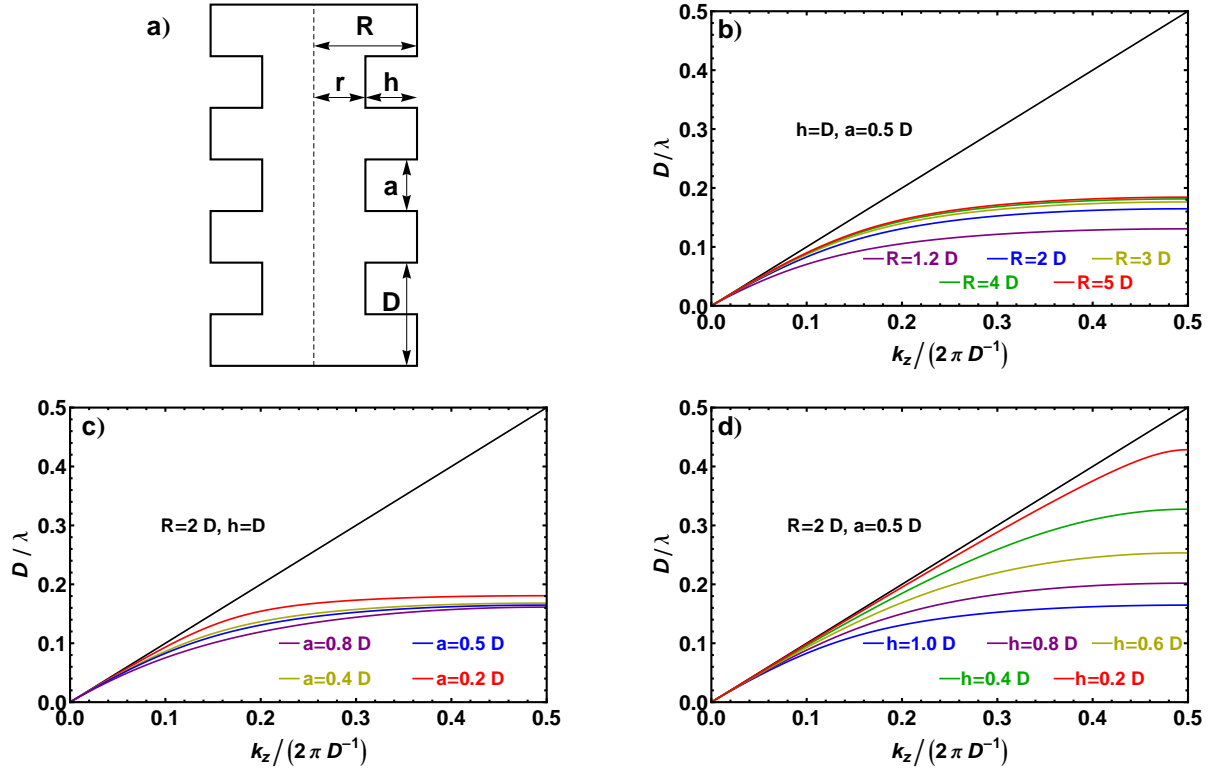


FIG. 1: a) Scheme of a corrugated wire with grating periodicity D , indentation width and depth a and h , respectively. R and $r=R-h$ are the outer and inner wire radius, respectively. b)-d) Dimensionless dispersion curves of the bound TM surface wave obtained as solutions to the implicit Eq.1 and parametrized by b) outer wire radius R , c) corrugation width a and d) indentation depth h . The surface wave propagates vertically along the wire surface in z -direction. For reference the dashed blue curve for $h=D$, $a=0.5D$, $R=2D$ is shown in each.

μm . This grating is then grafted onto the surface of a lossy gold tip onto which a sharp gold nanoantenna is planted. The field enhancement and confinement properties of this hybrid multiscale structure are analysed by means of finite-element method (FEM) based electromagnetic simulations.

II. METHODS

To find the proper/correct dimensions of corrugations that can confine and guide mid-IR electromagnetic radiation between 5.7 and 6 μm along a gold metal tip we will approach the problem as follows: In the first step, we calculate the dispersion relation of surface waves

propagating on an azimuthally corrugated perfect electric conducting (i.e. non-dissipative) wire of outer radius R , surface grating periodicity D , and indentation width and depth a and h , respectively (see. Fig. 1a)). To this end, we have to solve numerically the implicit equation [18]:

$$\sum_{n=-\infty}^{\infty} \frac{k_0}{q_n} \frac{K_1(Rq_n)}{K_0(Rq_n)} S_n^2 = -\frac{J_1(Rk_0)N_0((R-h)k_0) - J_0((R-h)k_0)N_1(Rk_0)}{J_0(Rk_0)N_0((R-h)k_0) - J_0((R-h)k_0)N_0(Rk_0)}, \quad (1)$$

with $k_0 = \omega/c = 2\pi\tilde{\nu}$, $q_n = \sqrt{k_n^2 - k_0^2}$ and

$$S_n^2 = \frac{a}{D} \text{sinc}^2 \left(\frac{k_n a}{2} \right), \quad (2)$$

where $k_n = k_z + n(2\pi/D)$ with k_z denoting the surface wave vector in z-direction (along the wire axis). K_m is the m-th order modified Bessel functions and J_m and N_m are the m-th order Bessel functions of the first and second kind, respectively. In order to ensure convergence for the numerical calculation of the SPP dispersion relation, we consider at least four diffraction orders in the modal expansion of Eq. 1 (see Ref. [21], Fig. 1). The behavior of the SPP dispersion within the first Brillouin zone (i.e. $0 \leq k_z \leq \pi/D$) in dependence of the geometrical parameters R , a and h is depicted in Figs. 1b)-d) with all length scales being rescaled by D . A stronger deviation of the dispersion curve from the light line and thus a stronger confinement of the SPP bands is achieved with decreasing R and increasing a and h .

The specific set of parameters appropriate for our purposes is a tradeoff between practicality and confinement. On the one hand, we want the width of indentations and protusions to be the same to give a nice symmetrical grating pattern, i.e. $a = 0.5 D$. On the other hand we want the spoof SPP band to display a strong deviation from the light line indicating a strong confinement of the electromagnetic radiation to the surface, i.e. $h = D$. The corresponding spoof SPP dispersion band exhibits an asymptotic limit at $0.165 = D/\lambda$. Since we want the asymptotic limit of the spoof SPP to appear at $1755 \text{ cm}^{-1} (\hat{=} 5698 \text{ nm})$ in order to provide good confinement of a surface wave at the lipid and protein absorption wavelengths, D has to be 940 nm, which is easily feasible with standard ion beam milling techniques.

With these specific dimensions for our grating ($D = 940 \text{ nm}$, $a = 470 \text{ nm}$ and $h = D$), we analyse by means of an electromagnetic solver based on the finite element method (JCMSuite by JCMWave GmbH) the field distribution around a $25 \mu\text{m}$ long, corrugated and lossy gold wire of outer radius $R = 2 D = 1.88 \mu\text{m}$ when electromagnetic radiation of wavenumber

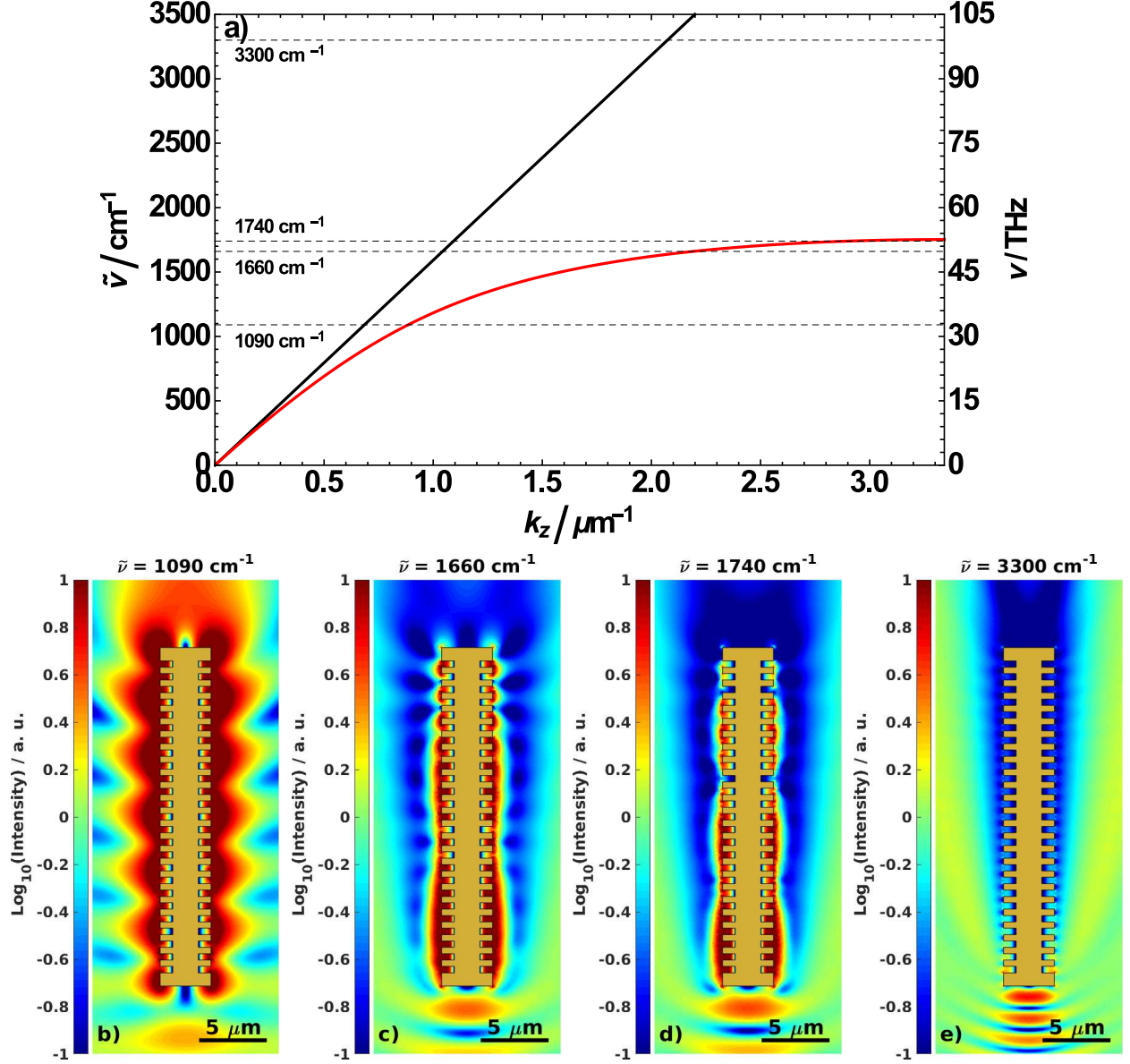


FIG. 2: a) Dispersion of a spoof SPP propagating along a surface grating with dimensions $D=940$ nm, $a=470$ nm and $h=940$ nm engraved onto a PEC wire with $3.76 \mu\text{m}$ in diameter. b)-e) Simulated electromagnetic field energy distribution along the surface of a lossy gold wire of same dimensions illuminated at the bottom by p-polarized light of wavenumbers 1090, 1660, 1740 and 3300 cm^{-1} .

1090 , 1660 , 1740 and 3300 cm^{-1} impinges in TM-mode (i.e. p-polarized with E-field parallel to the plane of incidence which coincides with the picture plane) from the bottom of the wire along its vertical axis. For the frequency dependence of the complex dielectric constant of gold, we used the Lorent-Drude model with parameters taken from Ref. [25]. According to the the spoof SPP dispersion curve belonging to our grating (Fig. 2a)), we expect an

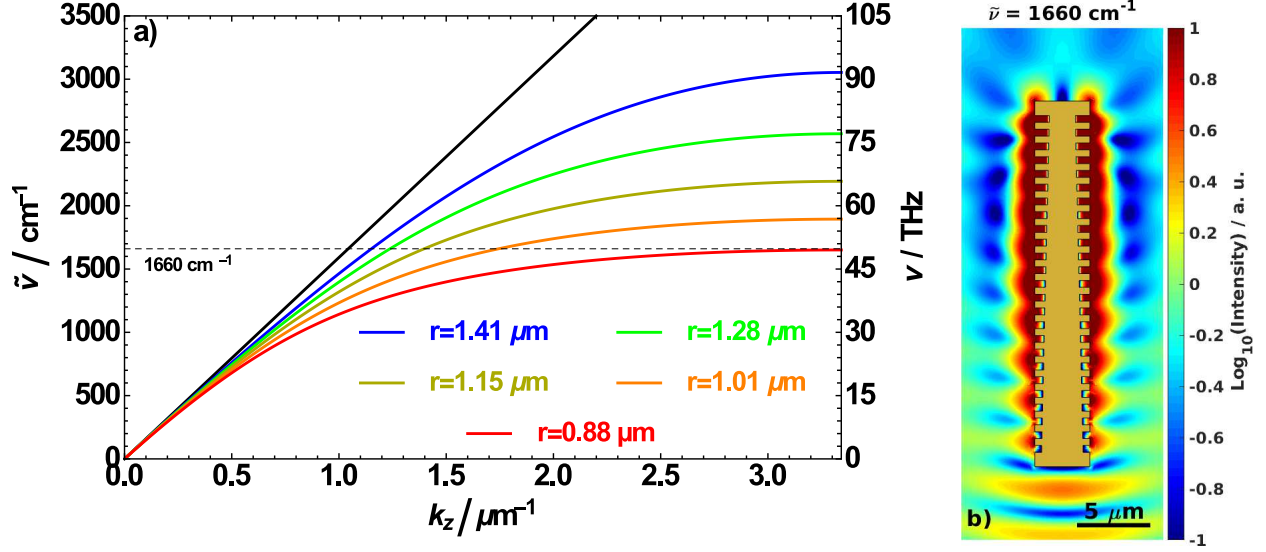


FIG. 3: a) Spoof SPP dispersion for a set of five PEC wires with different inner radius r . The residual wire and grating dimensions are kept the same as before. b) Simulated field energy of the spoof SPP mode excited at 1660 cm^{-1} and propagating along the surface of a lossy gold wire with the same dimensions as before except the inner radius r is continuously decreased from $1.41 \mu\text{m}$ at the bottom to $0.88 \mu\text{m}$ at the top of the wire. This illustrates the adiabatic compression of the surface field as it propagates in direction of decreasing inner radius.

increasing confinement of the surface waves as we approach the asymptotic frequency at 1755 cm^{-1} from the far-infrared end of the spectrum, and no excitation of spoof SPP waves at all in the near-infrared frequency range. This grating-induced field/wave dispersion is underpinned by the corresponding simulated field energy density plots, shown in logarithmic scale in Figs. 2b)-e). At 1090 cm^{-1} the surface wave extends far outside the region of the wire while they are tightly confined to the wire surface at 1660 cm^{-1} and 1740 cm^{-1} . At the near-infrared frequency of 3300 cm^{-1} , the grating cannot support surface waves and the incident radiation is already scattered at the bottom end of the wire.

Since a real s-SNOM experimental setup would not employ a corrugated wire as a probe, we need to replace the metal wire of radius R by a tapered tip that would need to efficiently guide and focus IR radiation as the electromagnetic fields travel along the surface grating towards the tip. This concept of adiabatic field compression is illustrated in Fig. 3a) which shows the spoof SPP dispersion curves for five different corrugated gold wires with the same grating parameters a and D and the same outer radius R as before, but different inner radii,

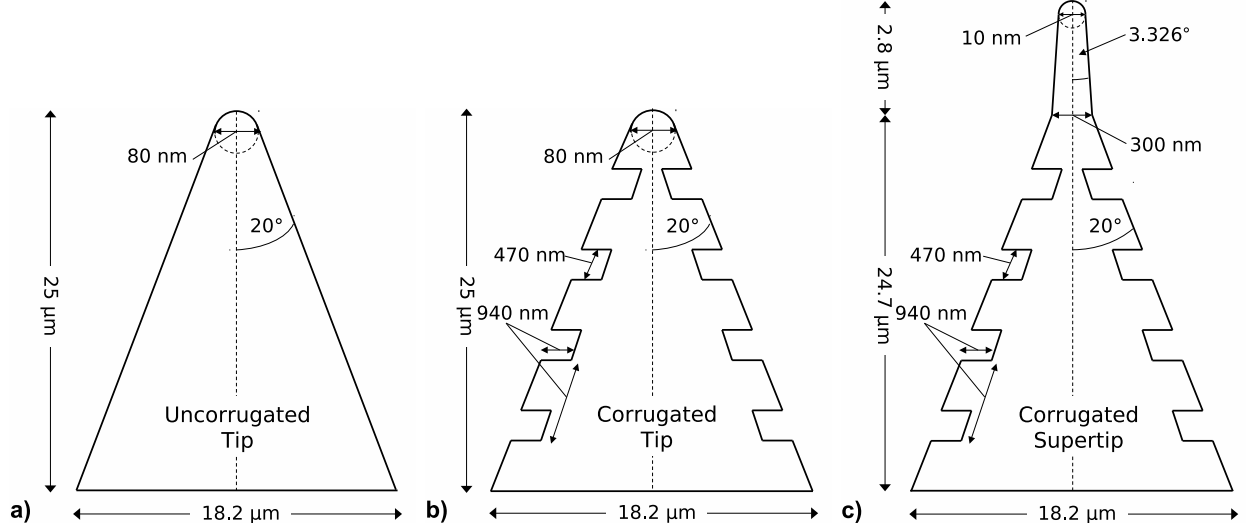


FIG. 4: Layouts of the near-field probes investigated in this work: a) An uncorrugated tip with dimensions of commercially available gold coated scanning probe microscopy tips typical used for IR s-SNOM (e.g. MikroMasch NSC16/CrAu). b) A corrugated tip of same dimensions as in a) but imprinted with a grating to support spoof SPPs at mid-IR wavelengths (see Fig. 2a)). c) A corrugated supertip composed of the corrugated tip fitted with a sharp apex for super resolution (see Ref.[6]).

$r=R-h$. The spoof SPP band at 1660 cm^{-1} supported on a wire with $1.41 \mu\text{m}$ inner radius (intersection between the dashed horizontal line and the blue solid line) is quite close to the light line and thus should extend over several wavelengths into the surrounding region, while on a wire with an inner radius of $0.88 \mu\text{m}$ where the asymptotic frequency lies around 1660 cm^{-1} , the spoof SPP band (intersection between the dashed horizontal line and the magenta solid line) is far from the light line and hence should be tightly confined to the wire surface. This behaviour is also reflected in Fig. 3b), which shows the simulated field energy density plot for a lossy gold wire at 1660 cm^{-1} with fixed outer radius and variable inner radius gradually decreasing from $1.41 \mu\text{m}$ at the bottom to $0.88 \mu\text{m}$ at the top of the wire. As the surface waves travel along the wire from bottom to top the gradual decrease of the inner radius is accompanied by a gradual reduction of the group velocity and accordingly an increase in the spatial confinement.

III. RESULTS AND DISCUSSION

In view of our aim of designing a plasmonic assisted IR near-field nanoprobe, we will now consider a rounded gold cone as displayed in Fig. 4a) with dimensions common to most IR scattering-based scanning near-field optical microscopy (IR s-SNOM) probes. In detail, the tip is $25\text{ }\mu\text{m}$ long with an full cone angle of 40° and a tip curvature radius of 40 nm . It has been shown that tips with an apex diameter of 80 nm can achieve a lateral optical resolution of about the same size[26]. Onto its surface we imprint our previously designed grating with dimensions $D = 940\text{ nm}$, $a = 0.5 D$, and $h = D$. In contrast to our previous illustration of adiabatic field compression, here we keep the groove depth fixed and gradually reduce the outer tip radius instead (Fig. 4b)). For this corrugated tip, we expect a higher field confinement but a field extent at the tip apex as big as with the uncorrugated version. In anticipation of this, we also consider a third structure, what we call a corrugated supertip (Fig. 4c)), where we fit a $2.5\text{ }\mu\text{m}$ long sharp apex on top of the corrugated cone. This gold nanoantenna has a base diameter of 300 nm , a full cone angle of 6.65° , and a curvature radius of 5 nm . Such an acute structure can be fabricated by electron-beam induced deposition and has been utilized to achieve sub- 10 nm resolution in the optical regime [6]. Due to the dimensions of our grating, it is not possible to corrugate the nanoantenna as well, so the grating does not stretch all the surface up to the apex.

To determine how these three different structures perform in terms of confinement, we conducted FEM electromagnetic simulations where all tips were illuminated from the base by a p-polarized plane-wave with a frequency of 1660 cm^{-1} , first at angle of incidence of 0° (Fig. 5, top row) and then at 75° (Fig. 5, bottom row) with respect to the tip axis, where the latter configuration has been used in all our previous experimental work [26–30] as well by others [31, 32]. The field energy density distribution is normalized by the field energy density of the incident light. At first glance, there is no field enhancement at 0° incidence, even though we see for the corrugated structures excitation of spoof SPPs that are strongly confined to the grating. By contrast, we observe a field confinement at the tip apex for an angle of incidence of 75° , which increases as we switch from the uncorrugated tip to the corrugated tip and then to the corrugated supertip.

Before we elaborate on the angular dependence of the field enhancement, we first quantify the field confinement as an assessment for the achievable optical lateral resolution. As a

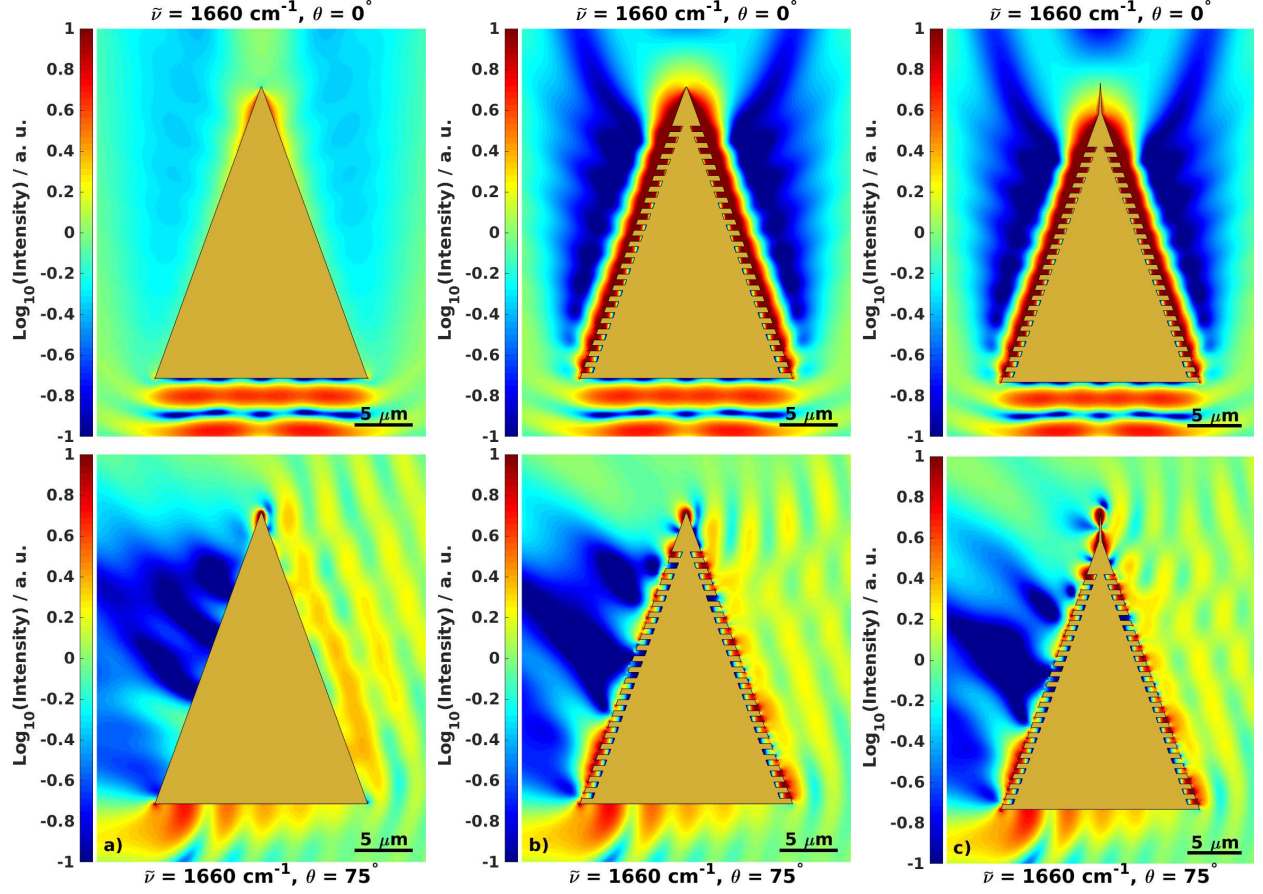


FIG. 5: FEM simulations of the electromagnetic field energy around the surface of a lossy a) uncorrugated gold tip, b) corrugated gold tip, and c) corrugated supertip, all excited by p-polarized light at 1660 cm^{-1} impinging from the bottom at an angle of 0° (top row) and 75° (bottom row) relative to tip axis.

measure we take the lateral field extent around the tip measured as the radial distance at which the field energy \tilde{r} starts to follow a different power law visible as kinks in Fig. 6a). Expecting the field extent to be comparable to the tip diameter we find the corrugated supertip to exhibit a sharp field distribution with a width of about 10 nm and a field enhancement of up to 3 orders magnitude larger compared to the ordinary tip, which provides a relatively poor lateral resolution of about 80 nm in agreement with the experimental findings mentioned earlier. Its corrugated counterpart provides the same lateral resolution, but about a factor of 2.5 better field enhancement thanks to the grating-induced SPPs.

Now, regarding the angular dependence of the field enhancement as depicted in Fig. 6b), the curve belonging to the uncorrugated gold tip features a multiple peaked, sloping

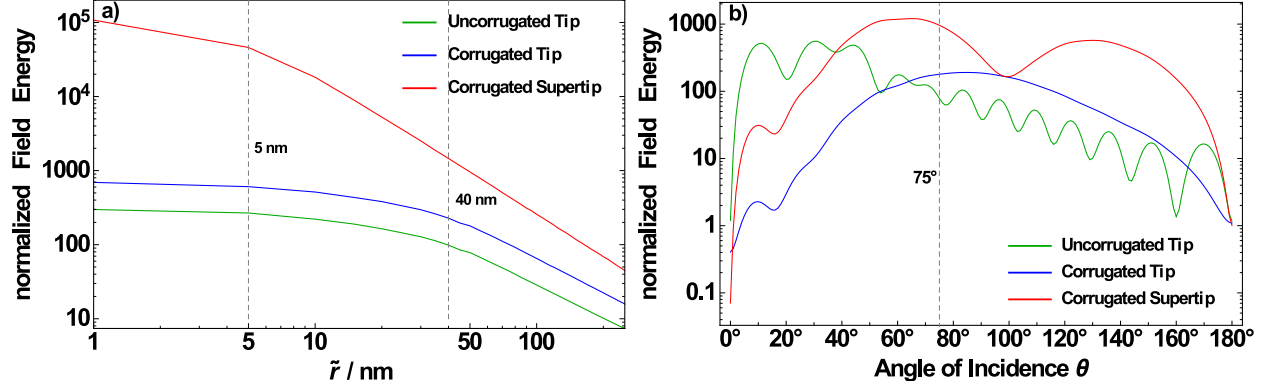


FIG. 6: a) Field energy as function of the radial distance from the tip apex in double logarithmic representation. The field confinement at the tip apex is measured as the extent at which the field drops down to $1/e$ of its value at the tip center (see dashed vertical lines). b) Field energy measured around the tip apex ($\tilde{r} = 50$ nm) of all three tip configurations as function of the angle of incidence. The dashed vertical line indicates the angle of incidence usually used in our experimental setup.

distribution with the maximum at 30° similar to the study in Refs. [33, 34]. In agreement with antenna theory [35], the peaks of the multiple lobe radiation pattern of a long wire of length l appear at angles of $\theta_m = \arccos[1 \pm (2m + 1) \lambda / (2l)]$ ($m = 0, 1, 2, \dots$). Thus, the major radiation lobe ($m = 0$) for a $25 \mu\text{m}$ long wire at an illumination wavelength of $\lambda = 6.024 \mu\text{m}$ (i.e. $\tilde{\nu} = 1660 \text{ cm}^{-1}$) is expected to appear at 28° .

Up to the angle of grazing incidence (i.e. 20°), the corrugated tip displays a similar angle dependence for the fields enhancement with the first peak around 15° , but unlike the uncorrugated tip we notice at grazing incidence a rise of a shoulder rather than a local minimum. This can be explained by the fact that at grazing incidence the incoming p-polarized light has no field component along the surface, only along the surface normal. Thus, there is no field component to feed the antenna but only a component to excite the SPP. Beyond grazing incidence the long-wire field pattern is overshadowed by a broad angular distribution with no distinct features reflecting the almost omnidirectional excitation of spoof SPPs on the grating reaching a poorly pronounced/weak maximum at about 85° , i.e. almost perpendicular to the wire axis.

In contrast, the field enhancement around the tip apex of the corrugated supertip becomes more distinctive with peaks at an angle of incidence of 65° and 130° and a local minimum inbetween around 100° . This is a result of the synergy of the antenna excitation and SPP

excitation arising from the juxtaposition of an antenna and a grating in this single structure. From a geometrical analysis of the field components, we would expect the field enhancement around the apex of the corrugated supertip to peak at 65° and 155° with a local minimum in between at 110° : Starting at grazing incidence where the electric field is entirely perpendicular to the surface, the ratio of the field components $E_{\parallel}/E_{\perp} = \tan(\theta - 20^\circ)$ shifts in favour of E_{\parallel} with increasing angle. At an angle of incidence of $\theta = 65^\circ$ (i.e. 45° relative to the tip surface) both field components, E_{\parallel} and E_{\perp} , are even and thus both effects (antenna excitation and SPP excitation) should coherently contribute to the field confinement at the tip apex. Beyond that angle, the ratio shifts even further in favour of E_{\parallel} until the electric field vector is entirely parallel to the surface at 110° allowing only the antenna effect to contribute. As the angle increases further, the ratio now starts to shift in favour of E_{\perp} and at 155° both field components are even again, thus maximizing again the cooperation of antenna and SPP excitation. However, our geometrical analysis does not entirely reproduce the observed angle distribution, particularly at obtuse angles, i.e. $\theta > 90^\circ$. There, the characteristics of the antenna with its sloping distribution become more prominent making the peak at 155° not only to appear at about 15° smaller angle, but also to have a smaller height compared with the peak at 65° . All in all, the angular distribution for the field enhancement of the corrugated supertip is a trade-off between the sharp dominant resonances of the long-wire antenna at acute and obtuse angles and the rather broad “resonance” of the grating at intermediate angles, reflecting the structural hybridisation of the antenna and the grating.

IV. CONCLUSION

By means of mode matching, we designed an experimentally feasible surface grating that excites spoof SPPs in the chemical fingerprint region between 5.7 and $6 \mu\text{m}$ (i.e. between 1660 and 1755 cm^{-1}). We grafted this grating onto the surface of a tapered metal waveguide structure to which we appended a nanoscale antenna with a 5 nm tip radius. FEM electromagnetic simulations revealed extraordinary field enhancement of 2-3 orders higher compared with conventional IR near-field probes. This field enhancement is accompanied by field confinement at the tip apex of the order of 10 nm holding the prospect of a fourfold increase in lateral optical resolution in comparison with conventional metal probes utilized

in current s-SNIM apparatus. A goniometric analysis of the field excitation revealed a broad range of angles under which extraordinary field enhancement can be achieved. Thus, implementation of the nanoprobe presented here into existing near-field IR microscopy apparatus should be possible with minor or no modifications. With such a plasmon-assisted mid-IR nanoscopy probe available the label-free imaging of single protein or lipid molecules within biological tissue is possible. Adapting the grating to the appropriate wavelength, such a probe can be also deployed to detect small fluctuations in the free carrier concentration of highly doped semiconductor nanostructures.

V. ACKNOWLEDGEMENT

The authors thank R. P. Zaccaria (IIT Genova) and E. DiFabrizio (KAUST) for fruitful discussions and S. Burger (JCMWave GmbH) for the technical support with JCMSuite. The authors also thank the BMBF for the financial support under grant no. 05K10PCA. F. Ballout greatly appreciates the financial support under the “Scheme to support special activities of doctoral students” granted by the rectorate of the Ruhr-Universiy Bochum. M. Havenith acknowledges the financial support Single Molecule Detection (SMD), a project funded by the EU Commission under the 7th Framework Programme.

-
- [1] A. J. Huber, D. Kazantsev, F. Keilmann, J. Wittborn, and R. Hillenbrand, *Advanced Materials*, **2007**, *19*, 2209.
 - [2] A. J. Huber, F. Keilmann, J. Wittborn, J. Aizpurua, and R. Hillenbrand, *Nano Letters*, **2008**, *8*, 3766–3770.
 - [3] A. J. Huber, J. Wittborn, and R. Hillenbrand, *Nanotechnology*, **2010**, *21*, 235702–235708.
 - [4] A. J. Babadjanyan, N. L. Margaryan, and K. V. Nerkararyan, *Journal of Applied Physics*, **2000**, *87*, 3785–3788.
 - [5] F. De Angelis, M. Patrini, G. Das, M. Galli, I. Maksymov, L. Businaro, L. C. Andreani, and E. Di Fabrizio, *Nano Letters*, **2008**, *8*, 2321–2327.
 - [6] F. De Angelis, G. Das, P. Candeloro, M. Patrini, M. Galli, A. Bek, M. Lazzarino, I. Maksymov, C. Liberale, L. C. Andreani, and E. Di Fabrizio, *Nature Nanotechnology*, **2010**, *5*, 67–72.

- [7] J.-B. Pendry, L. Martin-Moreno, and F.-J. Garcia-Vidal, *Science*, **2004**, *305*, 847.
- [8] F.-J. Garcia-Vidal, L. Martin-Moreno, and J.-B. Pendry, *Journal of Optics A*, **2005**, *7*, S97.
- [9] A. P. Hibbins, B. R. Evans, and J. R. Sambles, *Science*, **2005**, *308*, 670.
- [10] C. R. Williams, S. R. Andrews, S. A. Maier, A. I. Fernández-Domínguez, L. Martín-Moreno, and F. J. García-Vidal, *Nature Photonics*, **2008**, *2*, 175–179.
- [11] W. Zhu, A. Agrawal, and A. Nahata, *Optics Express*, **2008**, *16*, 6216–6226.
- [12] W. Zhao, O. M. Eldaiki, R. Yang, and Z. Lu, *Optics Express*, **2010**, *18*, 21498–21503.
- [13] F. J. García de Abajo and J. J. Sáenz, *Physical Review Letters*, **2005**, *95*, 233901.
- [14] Y. Chen, Z. Song, Y. Li, M. Hu, Q. Xing, Z. Zhang, L. Chai, and C. Y. Wang, *Optics Express*, **2006**, *14*, 13021–13029.
- [15] S. A. Maier, S. R. Andrews, L. Martin-Moreno, and F. J. Garcia-Vidal, *Physical Review Letters*, **2006**, *97*, 176805.
- [16] S. A. Maier and S. R. Andrews, *Applied Physics Letters*, **2006**, *88*, 251120.
- [17] Z. Ruan and M. Qiu, *Applied Physics Letters*, **2007**, *90*, 201906.
- [18] A. I. Fernandez-Dominguez, L. Martin-Moreno, F. J. Garcia-Vidal, S. R. Andrews, and S. A. Maier, *IEEE Journal of Selected Topics in Quantum Electronics*, **2008**, *14*, 1515–1521.
- [19] S. H. Yang and P. R. Bandaru, *Optical Engineering*, **2008**, *47*, 029001.
- [20] B. Wang, L. Liu, and S. He, *Journal of Applied Physics*, **2008**, *104*, 103531.
- [21] L. Shen, X. Chen, and T.-J. Yang, *Optics Express*, **2008**, *16*, 3326–3333.
- [22] L. Shen, X. Chen, Y. Zhong, and K. Agarwal, *Physical Review B*, **2008**, *77*, 075408 .
- [23] A. Rusina, M. Durach, and M. I. Stockman, *Applied Physics A: Materials Science & Processing*, **2010**, *100*, 375–378 .
- [24] N. Talebi and M. Shahabadi, *Journal of Physics D: Applied Physics*, **2010**, *43*, 135302.
- [25] A. D. Rakic, A. B. Djurišić, J. M. Elazar, and M. L. Majewski, *Applied Optics*, **1998**, *37*, 5271–5283.
- [26] I. Kopf, J.-S. Samson, G. Wollny, C. Grunwald, E. Bründermann, and M. Havenith, *Journal of Physical Chemistry C*, **2007**, *111*, 8166–8171.
- [27] J.-S. Samson, G. Wollny, E. Bründermann, A. Bergner, A. Hecker, G. Schwaab, A. D. Wieck, and M. Havenith, *Physical Chemistry Chemical Physics*, **2006**, *8*, 753–758.
- [28] G. Wollny, E. Bründermann, Z. Arsov, L. Quaroni, and M. Havenith, *Optics Express*, **2008**, *16*, 7453–7459.

- [29] M. Filimon, I. Kopf, F. Ballout, D. A. Schmidt, E. Bründermann, J. Rühe, S. Santer, and M. Havenith, *Soft Matter*, **2010**, *6*, 3764–3768.
- [30] F. Ballout, H. Krassen, I. Kopf, K. Ataka, E. Brndermann, J. Heberle, and M. Havenith, *Physical Chemistry Chemical Physics*, **2011**, *13*, 21432–21436.
- [31] L. Gomez, R. Bachelot, A. Bouhelier, G. P. Wiederrecht, S. Shih-hui Chang, S. K. Gray, F. Hua, S. Jeon, J. A. Rogers, M. E. Castro, S. Blaize, I. Stefanon, G. Lerondel, and P. Royer, *Journal of Optical Society of America B*, **2006**, *23*, 823–833.
- [32] S. C. Kehr, L. M. Yongmin, L. W. Martin, P. Yu, M. Gajek, S.-Y. Yang, C.-H. Yang, M. T. Wenzel, R. Jacob, H.-G. von Ribbeck, M. Helm, X. Zhang, L. M. Eng, and R. Ramesh, *Nature Communications*, **2011**, *2*, 249.
- [33] W. Krieger, T. Suzuki, M. Völcker, and H. Walther, *Physical Review B*, **1990**, *41*, 10229–10232.
- [34] M. J. Hagmann, *Journal of Vacuum Science & Technology B*, **1997**, *15*, 597–601.
- [35] C. A. Balanis, *Antenna Theory: Analysis and Design*; 3rd Edition; Wiley-Interscience; 2005.